Large-Scale Electromagnetic Turbulence Simulations with Kinetic Electrons from the Summit Framework

S.E. Parker 1), Y. Chen 1), B.I. Cohen 2), A.M. Dimits 2), W.M. Nevins 2), D. Shumaker 2), V. K. Decyk 3) and J. N. Leboeuf 3)

1) Univ. of Colorado, Boulder, Colorado, USA
2) Lawrence Livermore National Laboratory, Livermore, California, USA
3) Univ. of California, Los Angeles, California, USA

email contact: sparker@colorado.edu

Abstract. Results from gyrokinetic turbulence simulations including electromagnetic perturbations ($\delta \mathbf{B}_\perp$) and kinetic electrons in three-dimensional toroidal geometry with realistic tokamak plasma parameters are reported. This model includes electron-ion collisions and has been well benchmarked in the linear limit. It is found that for H-mode parameters, kinetic electrons increase the linear ITG growth rate and there is a corresponding decrease in the critical ion temperature gradient due to trapped-electron drive. However, a nonlinear up-shift in the critical gradient or a super-critical region still persists. The linear behavior of the zonal flow is little affected by kinetic electrons. This work is being carried out using the "Summit Framework." Progress on Summit, an open-source framework for both local and global, massively parallel gyrokinetic turbulence simulations with kinetic electrons and electromagnetic perturbations, is reported.

The physics of kinetic electrons and electromagnetic perturbations is currently a primary challenge in the simulation of magnetic fusion turbulence and transport. Until recently, the vast majority of three-dimensional gyrokinetic particle simulations with realistic geometry have used the adiabatic electron approximation[1, 2, 3, 4]. A new electromagnetic kinetic electron model that uses a generalized split-weight scheme [5], where the adiabatic part is adjustable, along with a parallel canonical momentum formulation has been developed[6]. This is done in three-dimensional toroidal flux-tube geometry including electron-ion collisional effects and has been linearly benchmarked with the continuum codes GS2 and GYRO[7, 8]. This new electromagnetic kinetic electron simulation efficiently resolves phase space by using particle-in-cell methods, uses realistic mass ratios and is well converged with a timestep only one-third smaller than that of equivalent adiabatic electron runs.

It is found that for H-mode parameters, kinetic electrons increase the linear ITG growth rate and there is a corresponding decrease in the critical ion temperature gradient due to trapped-electron drive. However, a nonlinear up-shift in the critical gradient or a super-critical region still persists [9]. Fig. 1 (A) shows the ion heat diffusivity as a function of R/L_T for a scan about the "Cyclone Base Case" parameters (which are typical H-Mode parameters from D-IIID [10, 9]) similar to the "U. Col." Scan in Ref. 8, except that electron-ion collisionality is included here. The critical gradient with kinetic electrons is $R/L_T = 4.5$, showing a super-critical region from $4.5 - 5$ with kinetic electrons.

Zonal flows play an important role in regulating the turbulence and transport[11]. However, the linear behavior of the zonal flow is little affected by kinetic electrons. Numerical studies of the effects of kinetic electrons on the evolution of the Geodesic Acoustic Mode

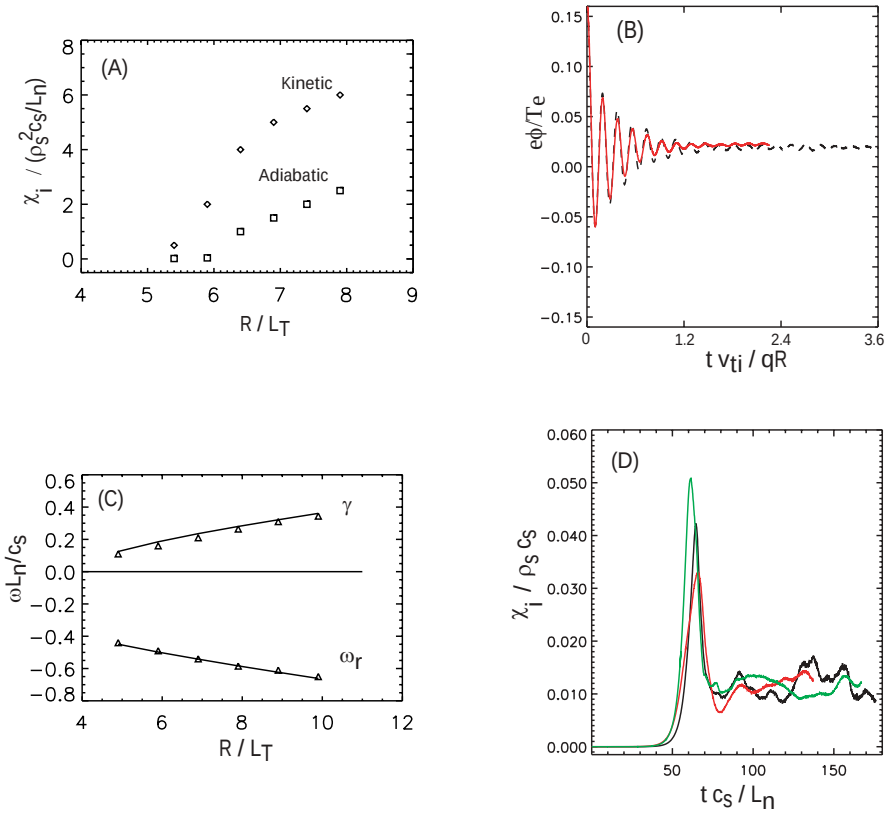

Figure 1: (A) R/L_T scan of the ion thermal diffusivity comparing fully kinetic electrons to adiabatic electrons. (B) Comparison of the zonal flow damping and residual level showing little difference between kinetic electrons (dashed) and adiabatic electrons (solid). (C) Linear benchmark with GS2[7] with with Cyclone Base Case parameters showing good agreement in mode growth rate and frequency. (D) Ion heat diffusivity versus time for three simulations with 8, 17 and 34 million particles, demonstrating good convergence properties of the simulation method.

(GAM) and the residual zonal flow[12] have been performed. Theory predicts no significant change due to kinetic electron effects[12]. Fig. 1 (B) shows the evolution of the GAM with kinetic electrons (the solid line) and adiabatic electrons (the dashed line). The initial damping rate of the GAM is slightly increased in the case of kinetic electrons, while the residual flow level not significantly changed. Little difference is found between adiabatic and kinetic electron models over a range of the safety factor q, which has been found to be important for determining the residual level [12].

Fig. 1 (C) shows a linear benchmark between Summit and GS2[7] of the most unstable mode varying R/L_T using Cyclone Base Case parameters. Fig. 1 (D) is a convergence study with respect to particle number. Base case runs with 8, 17, and 34 million particles are shown. The 34 million particle case has 64 particles per cell. This shows that the δf particle method appears to be well-converged within this range of parameters. Timestep and grid size convergence studies have also been carried out. Detailed parameters for the results presented in Fig. 1 (A)-(D) are given below.

Moderate-β simulations are reported in the poster presentation and are further docu-

mented in Ref.[13]. A complementary kinetic electron model based on closing zero-inertia drift-fluid equations has also been developed [14, 15], and progress is being made simulating electromagnetic turbulence using this model as well. The kinetic electron hybrid model is now running in three-dimensional toroidal flux-tube geometry and cross-checking with the fully kinetic model is underway. These algorithms address the physics regime of higher plasma β. Of particular interest are the competing effects of trapped electrons that increase instability and finite beta that is stabilizing in the regime where β is below the kinetic ballooning limit.

Methods for incorporating realistic magnetic equilibria and global effects using quasi-ballooning coordinates have been developed and implemented, and benchmarking between code versions is under way[16]. All the gyrokinetic simulation work reported here is being carried out jointly through a multi-institutional collaboration called the "Summit Framework." Summit is an open-source framework for both local and global massively parallel gyrokinetic turbulence simulations with kinetic electrons and electromagnetic perturbations [17]. This framework, written in Fortran 90, provides a unified object-based environment for sharing common components. Work is underway through Summit to include the kinetic electron models reported here, realistic magnetic geometry using quasi-ballooning coordinates [2] and global effects [16] under one software environment. This will allow the scientist to choose the physics components (and associated numerical advantages and disadvantages) most appropriate for the given problem at hand.

Three important analytical/numerical techniques are used to achieve vastly improved kinetic electron results. First, a canonical parallel momentum formulation is used to eliminate difficulties with obtaining a centered finite-difference for $\partial A_{\|}/\partial t$ in the evaluation of $E_{\|} = -\nabla_{\|}\phi + \frac{1}{c}\partial A_{\|}/\partial t$[18]. Second, an adjustable split-weight method is used for the electrons that permits larger timesteps[6]. Third, there is a careful numerical evaluation if the $\beta m_i/m_e A_{\|}$ term (described in more detail below) that appears in Ampere's law in the canonical parallel momentum formulation that permits accurate electromagnetic simulations at moderate β. The needed numerical techniques at moderate β and related simulation results are discussed in detail in Ref. [13]. Here, we by briefly describe the canonical momentum formulation, where $p_{\|\alpha} = v_{\|\alpha} + \frac{q_\alpha}{m_\alpha}\langle A_{\|}\rangle$ is used as a coordinate. The gyrokinetic equation is then

$$\frac{\partial f_\alpha}{\partial t} + \mathbf{v}_{\mathrm{G}\alpha}\cdot\nabla f_\alpha + \dot{p}_{\|\alpha}\frac{\partial f_\alpha}{\partial p_{\|}} = C(f_\alpha), \tag{1}$$

where $\alpha = i, e$. Here $\dot{p}_{\|\alpha} = \frac{q_\alpha}{m_\alpha}\tilde{\mathbf{b}}\cdot\nabla\langle\phi\rangle - \frac{\mu_\alpha}{m_\alpha}\tilde{\mathbf{b}}\cdot\nabla B + v_{\|\alpha}(\mathbf{b}\cdot\nabla\mathbf{b})\cdot\mathbf{v}_E + \frac{q_\alpha}{m_\alpha}\mathbf{v}_{\mathrm{G}\alpha}\cdot\nabla\langle A_{\|}\rangle$, $\mathbf{v}_{\mathrm{G}\alpha} = v_{\|\alpha}\tilde{\mathbf{b}} + \mathbf{v}_{\mathrm{d}\alpha} + \mathbf{v}_E$ is the guiding center velocity. $\tilde{\mathbf{b}} = \mathbf{b} + \frac{\langle\delta\mathbf{B}_\perp\rangle}{B}$, $\mathbf{v}_{\mathrm{d}\alpha} = \frac{v_{\|}^2 + v_\perp^2/2}{\Omega_\alpha B^2}\mathbf{B}\times\nabla B$ is the magnetic curvature and gradient drift, $\mathbf{v}_E = \langle\mathbf{E}\rangle\times\mathbf{b}/B$. The electrons are drift-kinetic due to the small electron gyroradius.

The ions are simulated using the usual δf method. Define $f_i = f_{0\mathrm{i}} + \delta f_i$ with $f_{0\alpha}$ the Maxwellian distribution in $p_{\|\alpha}$ ($\varepsilon_\alpha = m_\alpha(v_{\perp\alpha}^2 + p_{\|\alpha}^2)/2$), $f_{0\alpha} = \frac{n_{0\alpha}}{(2\pi)^{3/2}v_{\mathrm{t}\alpha}^3}e^{-\varepsilon_\alpha/T_\alpha}$.

A fraction of the adiabatic part of the electrons perturbed distribution function is treated separately in the split-weight scheme. Thus, we write $f_e = f_{0\mathrm{e}} - \epsilon_g e\phi\frac{\partial f_{0\mathrm{e}}}{\partial\varepsilon_e} + h$. The perturbed distribution function h evolves according to

$$\frac{dh}{dt} - C_L(f_e) \;=\; -\left(v_{\|e}\frac{\delta\mathbf{B}_\perp}{B} + \mathbf{v}_E\right)\cdot\nabla f_{0\mathrm{e}} - \dot{\varepsilon}_e\frac{\partial f_{0\mathrm{e}}}{\partial\varepsilon_e} + \epsilon_g e\left[(\frac{\partial\phi}{\partial t} + \mathbf{v}_{\mathrm{G}e}\cdot\nabla\phi)\frac{\partial f_{0\mathrm{e}}}{\partial\varepsilon_e}\right] \tag{2}$$

The electric potential ϕ and its derivative $\dot{\phi} = \partial\phi/\partial t$ are computed from the gyrokinetic Poisson equation[19],

$$n_{0\mathrm{i}}\frac{q_i^2}{T_i}\left(\phi - \tilde{\phi}\right) + \epsilon_g n_{0\mathrm{e}}\frac{e^2}{T_e}\phi = q_i\int \delta f_i \delta(\mathbf{R}+\rho-\mathbf{x})\, d\mathbf{R}\, d\mathbf{v} - e\int h\, d\mathbf{v} \tag{3}$$

and its derivative

$$n_{0\mathrm{i}}\frac{q_i^2}{T_i}\left(\dot{\phi} - \dot{\tilde{\phi}}\right) = -\nabla\cdot q_i\int f_i \mathbf{v}_{\mathrm{Gi}}\delta(\mathbf{R}+\rho-\mathbf{x})\, d\mathbf{R}\, d\mathbf{v} + \nabla\cdot e\int f_e \mathbf{v}_{\mathrm{Ge}}\, d\mathbf{v} \tag{4}$$

respectively. In Eq. 3 $\tilde{\phi}$ is defined as $\tilde{\phi} = \sum_{\mathbf{k}}\Gamma_0(k_\perp^2 v_{\mathrm{ti}}^2/\Omega_i^2)\phi_k \exp(i\mathbf{k}\cdot\mathbf{x})$. with $\phi = \sum_{\mathbf{k}}\phi_k\exp(i\mathbf{k}\cdot\mathbf{x})$. $\dot{\phi}$ and $\dot{\tilde{\phi}}$ are similarly defined.

The vector potential $A_\parallel$ is given by Ampere's law

$$\left(-\nabla_\perp^2 + \frac{\omega_{\mathrm{pe}}^2}{c^2}\right)A_\parallel = \mu_0\left(q_i\int \delta f_i v_\parallel \delta(\mathbf{R}+\rho-\mathbf{x})\, d\mathbf{R}\, d\mathbf{v} - e\int h v_\parallel\, d\mathbf{v}\right) \tag{5}$$

The $\omega_{\mathrm{pe}}^2/c^2 A_\parallel$ term in this equation comes from the zero-order distribution $f_{0\mathrm{e}}$ which is Maxwellian in $p_\parallel$. In a previous implementation of the split-weight scheme[6] that used Eq. 5 directly, it is found that at moderate β the Alfvén wave frequency and ITG mode growth rate deviate from the dispersion relation significantly. This problem has been solved recently by evaluating the $\omega_{\mathrm{pe}}^2/c^2 A_\parallel$ term using the same marker particles and the same scattering operation that is used for the h term in Eq. 5. The resulting numerical form of Eq. 5 is a matrix equation that has dependence on all of the particle coordinates (which are functions of time) and is three-dimensional. The detailed algorithm and higher β results are reported in Ref. [13]. The results shown in Fig. 1 are very low β cases that are essentially electrostatic and in this case no modification to Eq. 5 is necessary.

Finally, we describe details of the simulation and parameters used for the results shown in Figs. 1 (A)-(D). A zero-β circular equilibrium is assumed with $B(r,\theta) = 1 - \frac{r}{R_0}\cos\theta$. The field-line-following coordinates[20, 21] (x, y, z) are defined by $x = r - r_0$, $y = \frac{r_0}{q_0}(q\theta - \zeta)$ and $z = q_0 R_0\theta$. Here (r, θ, ζ) are the usual toroidal coordinates, R_0 is the major radius at the magnetic axis, r_0 is the minor radius at the center of the simulation domain, $q_0 = q(r_0)$ the safety factor. The size of the simulation box along the field line is $2\pi q_0 R_0$. Periodic boundary conditions are used in x and y, while the toroidal boundary condition [20, 21] is used in z.

In the following simulations we use the DIII-D base case parameters[10, 9]: $R_0\kappa_n = 2.2$, $T_i = T_e$, $r_0/R_0 = 0.18$, $q_0 = 1.4$, $\hat{s} = (r_0/q_0)(dq/dr) = 0.78$. Fig. 1 (C) shows the growth rate and frequency of the $k_y\rho_i = 0.3$ mode as a function of R/L_T. Also shown are the results from the GS2 code[7] with kinetic electrons. For the base case $R_0\kappa_{\mathrm{Ti}} = 6.9$, the linear growth rate with kinetic electrons is $\gamma L_n/c_s = 0.21$, compared with the adiabatic electron result $\gamma L_n/c_s = 0.12$. By selectively treating the passing electrons as adiabatic and the trapped electrons as kinetic, and vice versa, it is determined that the increase to the growth rate is due to the non-adiabatic effect of the trapped electrons. This justifies an approximation where only trapped electrons are treated kinetically. However, no such approximation is made here.

Fig. 1 (D) shows the evolution of the ion heat flux $\chi = \left\langle \int d\mathbf{v}\hat{\mathbf{r}} \cdot \mathbf{v}_E \frac{1}{2} m_i v^2 \delta f_i \right\rangle$ normalized by L_{Ti}, for three cases: (a) box size $L_x \times L_y = 64\rho_i \times 64\rho_i$, $4,194,304$ particles per species; (b) $L_x \times L_y = 128\rho_i \times 128\rho_i$, $8,388,608$ particles per species; (c) $L_x \times L_y = 128\rho_i \times 128\rho_i$, $16,777,216$ particles per species. Grid sizes are $\Delta x = \Delta y = \rho_i$, $\Delta z = L_z/32$. Time step $\omega_{\mathrm{ci}} \triangle t = 4$. $m_i/m_e = 1837$, $\beta = 1 \times 10^{-4}$, $\nu_{\mathrm{ei}}/\omega_{\mathrm{ci}} = 10^{-3}$, $\epsilon_g = 0.5$. One can see that convergence with respect to box size and particle number is achieved with a box size of $64\rho_i \times 64\rho_i$ and 32 particles per grid cell. The ion heat diffusivity is estimated to be $\chi_i L_n/\rho_i^2 v_{\mathrm{Ti}} \approx 4.5$, compared with that from adiabatic electron simulations, $\chi_i L_n/\rho_i^2 v_{\mathrm{Ti}} \approx 2.4$.

This work is part of the Summit Framework, Computational Center for the Study of Plasma Microturbulence, an Office of Fusion Energy Sciences, United States Department of Energy, Scientific Discovery through Advanced Computing (SciDAC) Project. Thanks to W. Dorland, J. Candy and R. Waltz for help with GS2 and GYRO linear benchmarks.

References

[1] S. Parker, W. Lee, and R. Santoro, Phys. Rev. Lett. **71**, 2042 (1993).

[2] A. Dimits, T. Williams, J. Byers, and B. Cohen, Phys. Rev. Lett. **77**, 71 (1996).

[3] R. Sydora, V. Decyk, and J. Dawson, Plasma Phys. Controlled Fusion **38**, A281 (1996).

[4] Z. Lin, T. Hahm, W. Lee, W. Tang, and R. White, Science **281**, 1835 (1998).

[5] I. Manuilskiy and W. W. Lee, Phys. Plasmas **7**, 1381 (2000).

[6] Y. Chen and S. E. Parker, Phys. Plasmas **8**, 2095 (2001).

[7] W. Dorland, F. Jenko, M. Kotschenreuther, and B. Rogers, Phys. Rev. Lett. **25**, 5579 (2000).

[8] J. Candy and R. Waltz, General Atomics Report GA-A23876, *to appear in J. Comput. Phys.*, (2002).

[9] A. Dimits et al., Phys. Plasmas **7**, 969 (2000).

[10] S. Parker, C. Kim, and Y. Chen, Phys. Plasmas **6**, 1709 (1999).

[11] P. Diamond and Y. Kim, Phys. Fluids B **3**, 1626 (1991).

[12] F. L. Hinton and M. N. Rosenbluth, Plasma Phys. Controlled Fusion **41** (1999).

[13] Y. Chen and S. Parker, *submitted to J. Comput. Phys.* (2002).

[14] B. I. Cohen, A. M. Dimits, W. Nevins, Y. Chen, and S. E. Parker, Phys. Plasmas **9**, 251 (2002).

[15] B. I. Cohen, A. M. Dimits, W. Nevins, Y. Chen, and S. E. Parker, Phys. Plasmas **9**, 1915 (2002).

[16] J. Leboeuf, V. Decyk, A. Dimits, and D. Shumaker, Int. Sherwood Fusion Theory Mtg. (2002).

[17] http://www.nersc.gov/scidac/summit .

[18] T. S. Hahm, W. W. Lee, and A. Brizard, Phys. Fluids **31**, 1940 (1988).

[19] W. W. Lee, Phys. Fluids **26**, 556 (1983).

[20] M. A. Beer, S. C. Cowley, and G. W. Hammett, Phys. Plasmas **2**, 2687 (1995).

[21] C. C. Kim and S. E. Parker, J. Comput. Phys. **161**, 589 (2000).